An MRI Method To Map Tumor Hypoxia Using Red Blood Cells Loaded with a pO_2-Responsive Gd-Agent

Enza Di Gregorio,[†,§] Giuseppe Ferrauto,[†,§] Eliana Gianolio,[†] Stefania Lanzardo,[†] Carla Carrera,[†] Franco Fedeli,[†] and Silvio Aime*[,†,‡]

[†]Department of Molecular Biotechnologies and Health Sciences, University of Torino, Torino 10126, Italy and [‡]IBB-CNR-UOS at the University of Torino, Torino 10126, Italy. [§]These authors contributed equally to this work.

ABSTRACT

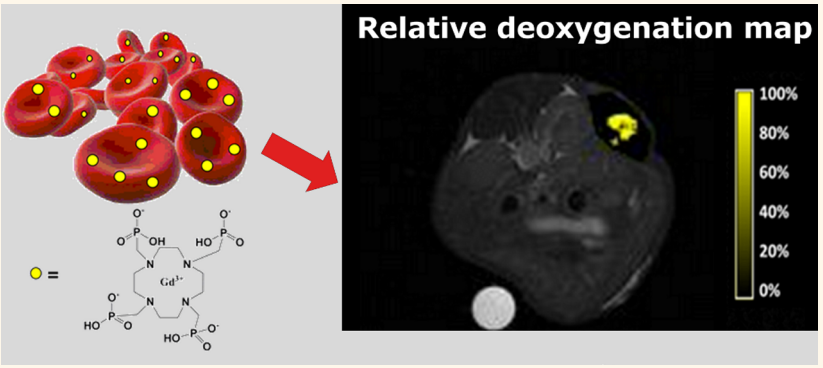

Hypoxia is a typical hallmark of many solid tumors and often leads to therapy resistance and the development of a more aggressive cancer phenotype. Oxygen content in tissues has been evaluated using numerous different methods for several imaging modalities, but none has yet reached the required standard of spatial and temporal resolution. Magnetic Resonance Imaging (MRI) appears to be the technique of choice and several pO_2-responsive probes have been designed for it over the years. *In vivo* translation is often hampered in Gd-relaxation agents as it is not possible to separate effects that arise from changes in local concentration from those associated with responsive properties. A novel procedure for the MRI based assessment of hypoxia is reported herein. The method relies on the combined use of Gd-DOTP- and Gd-HPDO3A-labeled red blood cells (RBCs) where the first probe acts as a vascular oxygenation-responsive agent, while the second reports the local labeled RBC concentration in a transplanted breast tumor mouse model. The MRI assessment of oxygenation state has been validated by photoacoustic imaging and *ex vivo* immunofluorescence. The method refines tumor staging in preclinical models and makes possible an accurate monitoring of the relationship between oxygenation and tumor growth.

KEYWORDS: magnetic resonance imaging · tumor hypoxia · red blood cells · contrast agents · vascular volume · Gd-DOTP

Hypoxia is one of the main tumor hallmarks and a characteristic feature of advanced solid tumors and results from an imbalance between oxygen supply and consumption.[1,2] In fact, tumor growth is often accompanied by heterogeneous vascular system growth leading to insufficient blood supply in some tumor regions, as oxygen's maximum diffusion distance is 70−150 μm, thus generating chronic hypoxia. Furthermore, intratumoral vascular networks are not well organized in cancers and severe structural and functional abnormalities are found. These include the formation of a chaotic architecture, which is characterized by an increase in vessels with an elongated and tortuous shape, the absence of flow regulation, intermittent stasis, high endothelial permeability and a lack of specific receptors. All these phenomena can lead to acute ischemic hypoxia, which is often transient.[3] The absence of sufficient oxygenation (either chronic or acute) can reduce the effectiveness of medical therapies. Radiotherapy, photodynamic therapy and many chemotherapeutic drugs which act on cell proliferation are active in well oxygenated regions, but have been found

* Address correspondence to silvio.aime@unito.it.

Received for review April 30, 2015 and accepted August 2, 2015.

Published online August 03, 2015
10.1021/acsnano.5b02604

to lack efficiency when tissue oxygen pressure (pO_2) is low.[4] Furthermore, cancer cells that lack sufficient O_2 show changes in gene expression and gene regulation pathways, leading to an alteration in the tumor cell proteome which permanently modifies cancer cell metabolism and aggressiveness.[5] The hostile environment triggers the selection and clonal expansion of more aggressive cancer cells that are able to survive in low or nil oxygen and nutrient supply conditions, thus generating a new cancer phenotype which is more aggressive and resistant to treatment.[6] The ability to assess hypoxia levels is central to cancer diagnosis and therapy for these reasons.[7,8] A direct measurement of pO_2 can be done using sensitive electrodes but this is not feasible in many cases.[9,10] Despite being able to provide a rapid and direct pO_2 measure, the resulting signal is very low, and more importantly, the technique is invasive and unsafe. Furthermore, internal organs cannot be reached, which limits the method to use on superficial cancers.[9,10] One of the "hot topics" in cancer research at present is the development of an imaging procedure that is able to determine pO_2 in the tumor region. Various imaging modalities, including optical, photoacoustic, Magnetic Resonance Imaging (MRI) and nuclear imaging, have been used to develop protocols for the detection of tumor hypoxia over the last few decades. Optical imaging is widely used in this field for the *ex vivo* characterization of tumor biopsies and for some preclinical *in vivo* studies. Several fluorescent probes, whose fluorescence is strongly quenched in the presence of O_2, have been proposed. However, a lack of penetration into in-depth regions is still a problem that strongly limits *in vivo* application to superficial cancers.[11] Progress has been made with recent developments in photoacoustic imaging (PAI) as it allows operators to selectively acquire images of oxy- and deoxy-Hemoglobin (Hb), thus providing detailed information on oxygenation state at greater depths than optical imaging.[12] As far as human applications are concerned, the gold standard is still nuclear medicine with Nitroimidazole (^{18}F-MISO) and other markers which are reduced in a hypoxic environment to yield species that are trapped inside hypoxic cells. Unfortunately, nuclear imaging's intrinsically low resolution has hampered pO_2-responsive tracers in clinical settings to some extent.[13,14] Meanwhile, MRI has been the focus of a great deal of attention as it combines well contrasted images of soft tissues, high in-depth penetration and a lack of ionizing radiation. Moreover, its high spatiotemporal resolution is all important when attempting to identify hypoxic and normoxic regions inside a tumor. Chemistry has also been playing an important role as it has developed innovative MRI contrast agents (CAs) which are able to detect parameters of physio/pathological interest for the characterization of both healthy and diseased tissues.[15,16] Some MRI procedures do not make use of CAs, but most *in vivo* applications rely on the use of the Blood Oxygen Level Depended (BOLD) approach.[17,18] This technique makes it possible to distinguish paramagnetic deoxy-Hb from diamagnetic oxy-Hb by observing signal intensity (SI) changes in T_2*-weighted proton images. One limitation is that the SI change is also strongly influenced by Hb concentration, which may be the result of a real variation in vascular volume and/or blood flow.[19] MRI contrast agent developers have long looked for new probes that can determine the oxygenation state of the microenvironment in which they distribute, *e.g.*, Mn (II−III)−Porphyrin complexes,[20] ^{19}F-based compounds,[21,22] and hyperpolarized agents.[23,24] However, these probes have not yet been tested *in vivo*. In 1995, our group investigated the *in vitro* relaxometric properties of [Gd(1,4,7,10-tetraazacyclododecane-*N*,*N*′,*N*″,*N*‴-tetrakis(methylenephosphonate))]$^{5-}$ Gd-DOTP[25−27] upon its binding with oxy- or deoxy-Hb[28,29] and reported that this molecule appeared to be suitable as a hypoxia reporter. In the meantime, new important advances in the loading of small molecules inside red blood cells (RBCs) have been made and have prompted us to further investigate the feasibility of using Gd-DOTP-labeled RBCs for *in vivo* applications.[30−32]

The MRI method that we present herein is based on the combined use of Gd-DOTP- and [Gd(10-(2-hydroxypropyl)-1,4,7-tetraazacyclododecane-1,4,7-triacetate] Gd-HPDO3A-labeled-RBCs, where the first probe acts as a vascular oxygenation-responsive agent and the second furnishes local labeled RBC concentration, for the evaluation of hypoxia in a transplanted breast tumor mouse model. The significance of this work lies in the possibility of developing a protocol that can achieve the high resolution, *in vivo* evaluation of tumor hypoxia in all of the body's organs. This method may also be of great interest from the preclinical point of view as it could be used to evaluate new therapeutic oncology protocols. Moreover, a future clinical transition may also be possible as the technique could become an aid in choosing suitable therapy; ineffective, harsh and expensive treatments can be avoided when the required tissue oxygenation conditions are not present.

RESULTS AND DISCUSSION

***In Vitro* Relaxometric characterization of Gd-Complexes.** Gd-DOTP (Figure 1A) is known to be a probe that can bind Hb. Furthermore, it has been proven that it has different binding affinities for the two Hb states; the presence or absence of O_2 (R and T state, respectively).[25−29] Its relaxivity increases upon Hb binding, mainly as the result of an increase in the rotational correlation time. This property links nicely with the idea of its loading inside RBCs to report on pO_2 once injected in the blood. In the case of tumors, it is expected that the change in SI in the region of interest can be correlated

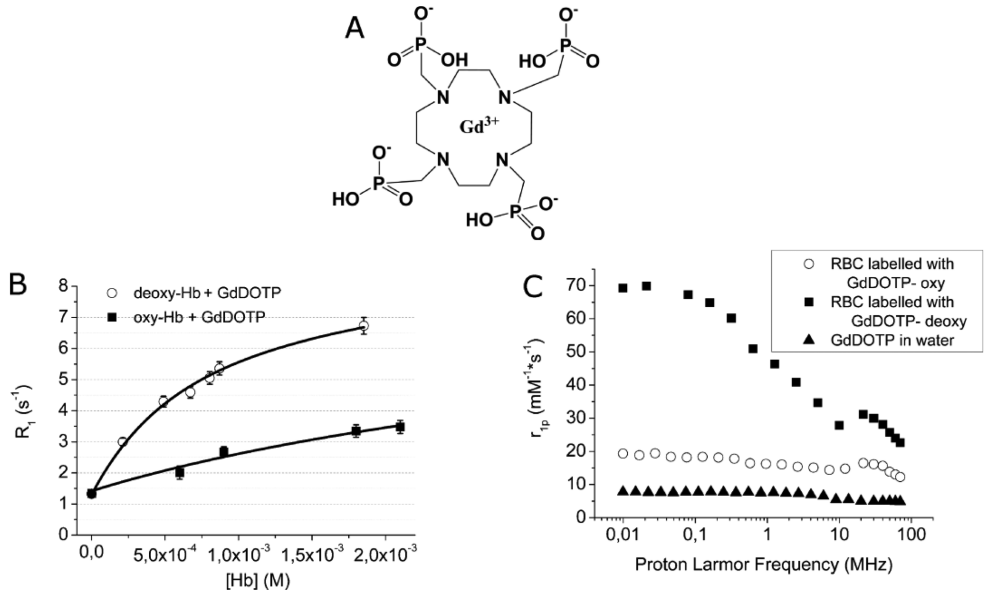

Figure 1. Gd-DOTP characterization. (A) Chemical structure of Gd-DOTP; (B) relaxometric titration of Gd-DOTP with oxy- or deoxy-Hb (mean ± SD); (C) NMRD profiles of Gd-DOTP-labeled RBCs in the presence of oxy- or deoxy-Hb and aqueous solution of Gd-DOTP.

to the actual oxygen pressure. The affinity constants (K_a) for the two Hb states were evaluated. Different concentrations of Hb, freshly extracted from mouse blood (in the presence of the endogenous concentration of 2,3 biphosphoglycerate (2,3 BPG)), were incubated with Gd-DOTP (0.1 mM) and the longitudinal relaxation rate ($R_1 = 1/T_1$) measured at 21.5 MHz and 25 °C (Figure 1B). The measured K_a and r_1-bound (*i.e.*, the relaxivity of the Gd-complex bound to the macromolecule) are reported in Table1. The number of binding sites was fixed at 1 per tetramer as previously established.[25−27] In accordance with a previously reported investigation,[25−27] Gd-DOTP displays high affinity for deoxy-Hb and a lower value for oxy-Hb (5 times higher for the former than for the latter). The affinity constant for deoxy-Hb measured here is slightly lower than the value reported in ref 16 ($K_a = 3300\ M^{-1}$) as this paper's binding experiment was carried out in the presence of the endogenous concentration of 2,3 BPG, which most likely acts as a competitor. The relaxation enhancement achieved is remarkable; the deoxy-Hb/Gd-DOTP adduct gives a relaxivity of 37.5 $mM^{-1}\ s^{-1}$, which is more than seven-times higher than the relaxivity of free Gd-DOTP (4.8 $mM^{-1}\ s^{-1}$). Gd-DOTP was then loaded inside RBCs using Hypotonic Swelling methodology,[33] *i.e.*, by subjecting the cells to an osmotic shock that makes the membrane transiently permeable to the compounds present in the incubation medium. A high amount (Figure S1) of Gd-DOTP can be loaded inside each cell using Hypotonic Swelling without any appreciable adverse effects (high cell recovery after treatment and low hemoglobin release). The relaxometric properties of the Gd-labeled RBCs were investigated by acquiring Nuclear Magnetic

TABLE 1. Values of the Binding Parameters of Gd-DOTP and Gd-HPDO3A toward Oxy-Hb and Deoxy-Hb Measured by Relaxometric Titrations at 21.5 MHz, 25 °C, and pH = 7.4

	Gd-DOTP	Gd-HPDO3A
K_a oxy-Hb (M^{-1})[a]	360 ± 150	104 ± 5.7
K_a deoxy-Hb (M^{-1})[a]	1823 ± 253	88 ± 6.5
r_b oxy Hb (s^{-1})	22.9 ± 10.5	n.a.
r_b deoxy Hb (s^{-1})	37.5 ± 1.77	n.a.
Ratio K_a deoxy/K_a oxy	5.1	0.85

[a] Values of K_a are expressed per tetramer.

Relaxation Dispersion (NMRD) profiles over an extended range of Larmor frequencies (0.01−80 MHz). NMRD profiles give a sort of molecular fingerprint of the paramagnetic complex that provides insight into the cellular microenvironment and possible relationships with other molecules. The profiles were acquired in both normoxia and oxygen deprivation conditions, which were obtained by removing O_2 from the specimen with the inflow of N_2 gas (Figure 1C). The occurrence of oxy- or deoxy-Hb was checked by recording a UV−vis Absorption Spectra of the samples (Figure S2). A relaxivity peak is present in the NMRD profiles at 30−40 MHz, typical of the interaction of the Gd-complex with a slowly moving macromolecule, for both Hb states. The relaxivity of labeled RBCs in hypoxic conditions is far higher than in normoxia over the entire investigated frequency range because of the higher interaction strength between Gd-DOTP and deoxy-Hb. It has been suggested that Gd-DOTP binds the protein at the site normally recognized by the allosteric effector 2,3 BPG *via* an interaction with the phosphonic

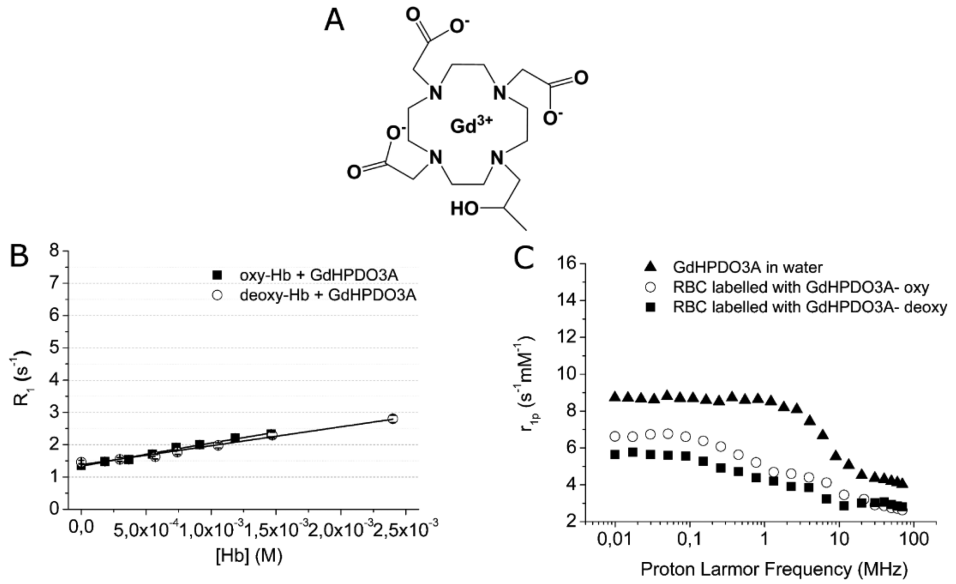

Figure 2. Gd-HPDO3A characterization. (A) Chemical structure of Gd-HPDO3A; (B) relaxometric titration of Gd-HPDO3A with oxy- or deoxy-Hb (mean ± SD); (C) NMRD profiles of Gd-HPDO3A-labeled RBCs (oxy and deoxy) and aqueous solution of Gd-HPDO3A.

groups with positively charged amino acids on the Hb β-chain.[25]

Gd-HPDO3A (ProHance, Bracco Imaging Spa, Figure 2A) was chosen to report on the local Gd-labeled RBC concentration. This uncharged and hydrophilic Gd-complex is well tolerated by cell machinery[32,34] and is used here as a contrast molecule that does not bind Hb regardless of whether it is in the T or R state. Its binding affinity constant (K_a) is practically negligible for both deoxy- and oxy-Hb (Figure 2B and Table1) as the observed increase in R_1 simply reflects the change in the viscosity of the solution upon increasing the Hb-concentration.

The absence of binding to Hb or any other intracellular macromolecules was confirmed *via* the acquisition of Gd-HPDO3A-labeled RBC NMRD profiles. Gd-HPDO3A were efficiently loaded inside RBCs *via* hypotonic swelling (Figure S1) and the Gd-HPDO3A-loaded-RBC NMRD profiles did not show any relaxation enhancement at 30−40 MHz (Figure 2C), whether in normoxic or hypoxic conditions. The relaxivity was actually lower than the value measured in water. This behavior may be ascribed to the well-known relaxivity quenching effect that occurs when large numbers of Gd-complexes are loaded inside cells.[35−37] In summary, Gd-HPDO3A-RBCs do not appear to react to changes in pO_2, while Gd-DOTP-RBCs are good reporters of the oxy-Hb/deoxy-Hb ratio.

O_2-Binding Affinity of Gd-DOTP-Labeled RBCs. Photoacoustic images (PAI) were acquired on tumor bearing mice pre and post Gd-DOTP-RBC administration in order to check whether the loading of RBCs with Gd-DOTP affected cell functionality (*i.e.*, O_2-binding). In PAI, nonionizing laser pulses are delivered into biological tissues, absorbed by an excitable molecule

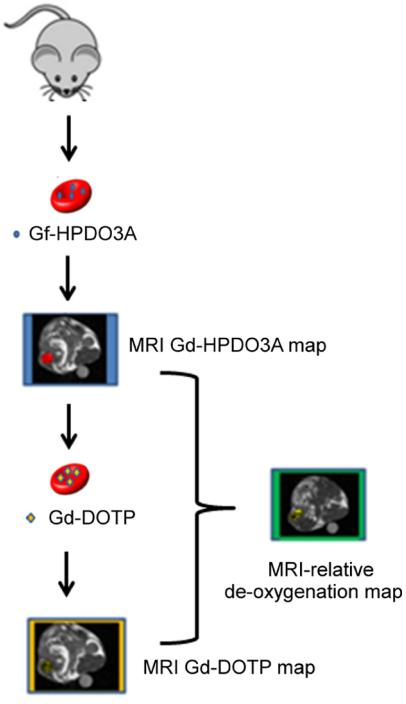

Figure 3. Illustrative scheme of the experimental setup. RBCs taken from the mouse are labeled with Gd-DOTP or Gd-HPDO3A. Gd-HPOD3A-RBCs are injected into the mouse tail vein and MRI vascular volume (V_v) maps are acquired. Then, Gd-DOTP-RBCs are injected into the same mouse and T_{1w} maps are acquired. The ratio between these two maps allowed us to obtain the relative MRI deoxygenation maps that report O_2 content independently of vascular volume.

(such as Hb) and converted into heat. This leads to a transient thermoelastic expansion and then to ultrasound emission that can be used to generate images. The Hb absorption spectrum differs with oxygenation and therefore dual-wavelength (750 and 850 nm) PAI

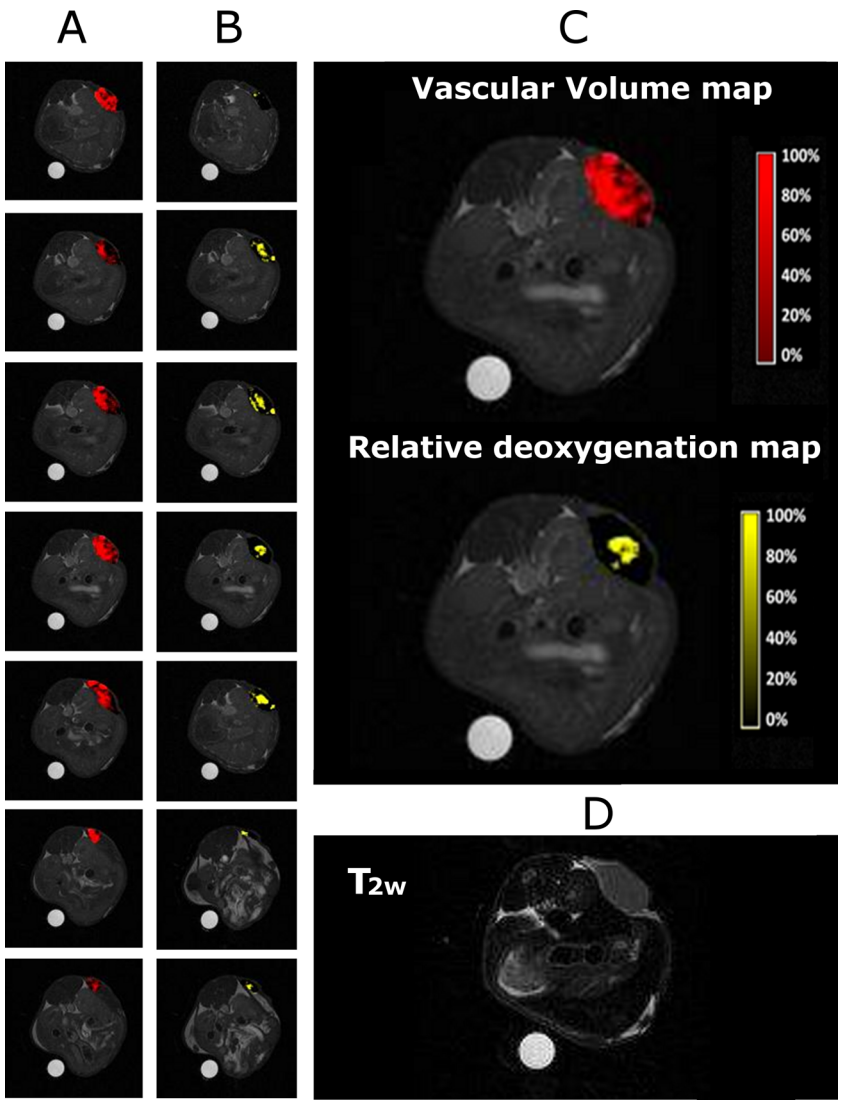

Figure 4. Vascular Volume and Relative deoxygenation maps of a representative tumor. (A) Vascular volume maps of 7 slices covering the tumor; (B) relative deoxygenation maps of 7 slices covering the tumor; (C) magnification of vascular volume (top) and relative deoxygenation (bottom) maps of the central slice of tumor; (D) T_{2w} image of the central slice of tumor.

acquisition can be used to selectively visualize and quantify oxy- and deoxy-Hb. A large number of superficial tissue and subcutaneous transplantable tumor applications have been reported for PAI in recent years.[38,39] PAI allows scientists to calculate hemoglobin oxygen saturation (SO_2), which is defined as the ratio between Oxy-Hb and total Hb concentrations 1:

$$SO_2 = \frac{[\text{Oxy-Hb}]}{[\text{Oxy-Hb}] + [\text{Deoxy-Hb}]} \quad (1)$$

The *in vivo* mapping of hypoxia was carried out on tumor transplanted models that were obtained *via* the subcutaneous injection of a murine mammary adenocarcinoma cell line (TS/A) into BALB/c mice.[40] Mean PAI SO_2 measurements in the tumor region, acquired both before and after Gd-DOTP-RBC administration, rule out the possibility that labeled-RBCs have any significant effect on oxygen saturation inside cells (Figure S3), as the pre and post SO_2 values are not significantly different (Paired Student's *t*-Test: $t(5) = 0.870$, $p = 0.424$). Analogously, no difference in SO_2 was noted upon the administration of Gd-HPDO3A-RBCs (data not shown).

***In Vivo* Experimental Setup for Vascular Oxygenation Measurement.** The use of Gd-DOTP-labeled RBCs alone in MRI experiments is not sufficient for the determination of oxygenation state in tumor voxels because of the MRI signal's dependence on CA-concentration. Therefore, the two agents (Gd-DOTP- and Gd-HPDO3A-labeled RBCSs) were used in combination, where the latter acts as a reporter of the local concentration of Gd-labeled RBCs (*i.e.*, of the vascular volume).

The experimental setup scheme is shown in Figure 3. It is made up of three steps; (i) the injection of Gd-HPDO3A- RBCs and MRI acquisition, (ii) the injection of Gd-DOTP-RBCs and MRI acquisition, and (iii) the

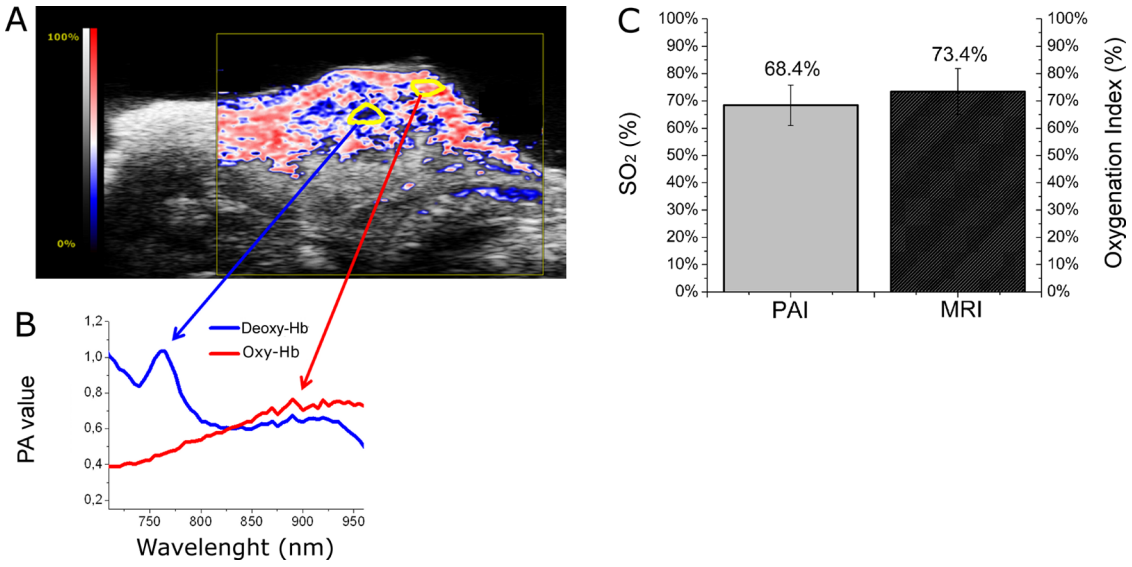

Figure 5. (A) PA image of central tumor slice showing hypoxic (blue) and normoxic (red) regions. (B) Spectra of deoxy and oxy-Hb acquiring by drawing ROI in tumor core and rim, respectively. (C) Mean values of oxygen content measured by MRI and PAI in the entire tumor.

ratiometric analysis of MR images which provided the signal enhancement (SE%) ascribable to deoxy-Hb. The T_{1w} images of TS/A tumors acquired upon Gd-HPDO3A-RBCs injection were used to give images in which SE does not depend on O_2 content and thus report, voxel by voxel, the vascular volume.[32]

Conversely, observed SE is dependent on both vascular volume and relative oxy-/deoxy-Hb concentration (related to actual SO_2 value) in the T_1w images of TS/A tumors acquired upon Gd-DOTP-RBC injection. The ratio between the two images allows data normalization which gives a map where signal intensity (SI) is not dependent on actual vascular volume but only on oxy- and deoxy-Hb content. The tumor was investigated by acquiring 7 parallel axial slices (slice thickness = q1 mm) that cover the entire tumor region (Figure 4). Each labeled-RBC administration was preceded by the withdrawal of an amount of blood which contained as many RBCs as there were labeled RBCs to be injected. This was done to keep the hematocrit value constant.

Representative images obtained upon Gd-HPDO3A-RBC administration are reported in Figure 4A. These maps report on vascular volume distribution voxel by voxel. The vascular network appears to be heterogeneously distributed within the tumor, although there are some poorly vascularized regions. GdDOTP-RBCS were successively (*ca.* 20 min after Gd-HPDO3A RBC injection) administrated and a new MRI acquisition was carried out. The vascular volume in each voxel was normalized which allowed the oxygenation maps to be calculated. The results are reported in Figure 4B. Higher levels of deoxy-Hb are highlighted by the presence of intense yellow areas in the ratiometric map. Conversely, darker voxels indicate areas of higher oxygenation. It should be noted that deoxy- and oxy-regions are not homogeneously distributed in the tumor mass. The internal regions are characterized by a strong deoxygenation profile, while the peripheral regions show no sign of hypoxia. An average vascularization of 10.6 $\pm$ 3.2% and an average relative oxygenation index of 73.4 $\pm$ 8.4% were measured over the entire tumor. The latter index should not be taken as a quantitative measure of the oxygen content of the tumor, but rather should be seen as qualitative and very useful when comparing different regions within a given tumor as well as different stages in tumor progression.

In Figure 4C (top, vascular volume map; bottom, hypoxia weighted map), it is well evident that the hypoxic region is largely dominant in the tumor core. The use of the proposed method to evaluate tissue hypoxia relies on the assumption that Hb oxygenation is proportional to blood pO_2 which, in turn, is in equilibrium with oxygen present in the surrounding tissues. In the tumor region, the oxygen tension may be low for two main reasons, namely (i) the tumor cells are consuming O_2 more rapidly than it can be delivered or (ii) the region is necrotic, thus there is less delivery because of the reduced vascularization. The latter case is ruled out because the T_{2w} image did not show necrosis (Figure 4D); thus, the areas showing an increase in deoxy-Hb can be accounted for the presence of cells characterized by a higher oxygen consumption.[41,42]

PAI and Microscopy Validation of MRI Results. PAI of the same mice was carried out in order to validate the MRI results. As shown in Figure 5, PAI indicates that the tumor core is more hypoxic than the rim. The different oxygenation levels may be more fully appreciated by looking at the colored map, reported in Figure 5A

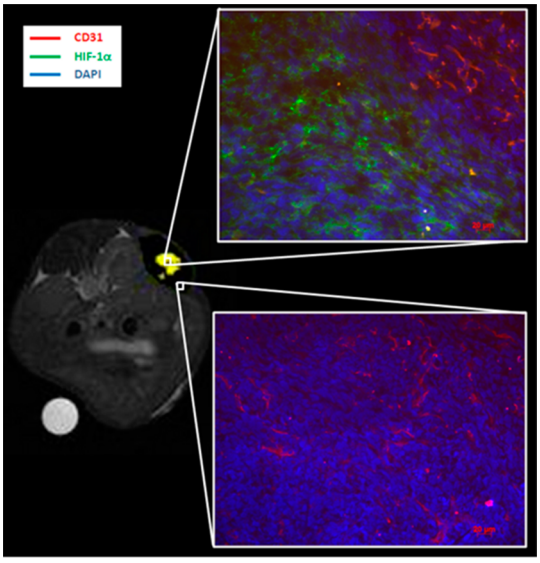

Figure 6. Immunofluorescence staining. Fluorescence image of a representative central slice of TS/A tumor reported in Figure 5. IF staining for CD31 (red) and HIF-1a (green). Nuclei were counterstained with DAPI (blue). Upper IF image is taken from tumor core; lower IF image is taken from tumor rim.

(red = highly oxygenated regions; blue = poorly oxygenated regions), and the corresponding PA spectra (Figure 5B). Total Hb distribution in the tumor region is reported in Figure S4A. PA images confirm the heterogeneous vascular network distribution that was detected by MRI. Moreover, the oxygenation levels that were measured by MRI and PAI over the entire tumor are compared in Figure 5C. There is good overall agreement between the two sets of measurements (oxygenation index (OI) % = 73.4 ± 8.4% by MRI *vs* SO_2 = 68.4 ± 7.5% by PAI, respectively) even if these two values cannot be directly compared as they are not defined in the same way. Further insight can be obtained by looking at the vascular oxygen content in the different tumor regions (by means of the two imaging modalities). Vascular oxygen content has been plotted against distance from the tumor center and is reported in Figure S4B; both the techniques highlight a progressive increase in oxygenation from the tumor core to the rim. This is in line with expectations that the tumor core is poorly oxygenated. Mice were sacrificed after *in vivo* imaging while the tumors were explanted and stained for vessels (CD31) and hypoxia (HIF-1α) markers. The tumor core is characterized by a large hypoxic region (Figure 6, upper inset). Conversely, there are no HIF-1α positive regions in the tumor rim (Figure 6, lower inset).

To further explore the potential of the method reported herein, murine breast tumors were compared at two different stages of their development; at an early and late stage when tumor sizes were 55 ± 5 and 130 ± 10 mm^3 (*i.e.*, 6 and 9 days after the tumor implantation). It is well-known that a change in vascular volume and oxygenation occurs during tumor growth. MRI shows the nonhomogeneous distribution of deoxy- and oxy-regions and of vascularised voxels at both tumor stages. An increase in vascular volume was observed upon the increase in tumor size (from 8.2 ± 0.7% to 16.7 ± 0.9%, Table S1). However, the growing vascular network does not provide enough O_2 to the entire tumor mass and the mean oxygenation index in the tumor decreases in the latter stage tumor (from 95.8 ± 2.5% to 73.0 ± 6.8%) (Figures S5 and S6, Table S1). Both the early and late tumor stage changes in vascular volume and oxygenation index can be considered significant ($P < 0.001$).

CONCLUSIONS

In summary, it has been shown that the pO_2-responsive properties of Gd-DOTP are maintained *in vivo* when the paramagnetic complex is entrapped in RBCs. Maps that report the actual deoxy-Hb/oxy-Hb ratio have been obtained. Gd-labeled RBCs appear to be safe, morphological and physiological analogues to native cells, while their complete retention in the vascular system means that tumor vascular volume and oxygen content can be evaluated. These important cancer hallmarks are strictly linked to disease development and malignance degree and their assessment *via* a high resolution imaging modalities, such as MRI, is undoubtedly of interest for characterizing tumor phenotype. In our opinion, both tumor staging and treatment follow-up can be greatly improved by evaluating hypoxia with this minimally invasive imaging method. Finally, the information on vascular oxygenation level obtained using this MRI method is in line data from PAI, which is restricted to superficial tissues only.

METHODS

Chemicals. Gd-HPDO3A was kindly provided by Bracco Imaging S.p.A (Colleretto Giacosa, Torino, Italy). Gd-DOTP was synthesized as reported elsewhere.[43] Fetal bovine serum (FBS), Roswell Park Memorial Institute-1640 (RPMI-1640) medium, glutamine, Pen/Strep solution and trypsine were purchased from Lonza Group. Ficoll Hystopaque, heparin and all other chemicals were purchased from Sigma-Aldrich Co. LLC.

Isolation of RBC and Labeling by Hypotonic Swelling. Erythrocyte separation was carried out using the Ficoll Hystopaque[10,39] methodology. Blood, diluted 1:1 with phosphate buffered saline (PBS), was stratified into Ficoll Hystopaque1039 and centrifuged for an uninterrupted 30 min at 1500 rpm and 25 °C. The pellet (containing erythrocytes) was separated from the other components, washed three times with Heparin supplemented PBS and centrifuged at 2300 rpm for 10 min and 4 °C. The separated erythrocytes were later used for uptake experiments. The labeling was carried out by loading the two Gd-complexes using the osmotic swelling methodology. Cells were placed in a hypotonic solution (160 mOsm/L) containing the CA to be

loaded (Gd-HPDO3A 100 mM or 20 mM or Gd-DOTP 20 mM), at 4 °C for 30 min. The isotonic condition (280 mOsm/L) was then restored by adding the necessary amount of phosphate buffer saline (PBS). The difference in the concentrations of the two Gd-complexes used depends on the different net charge of the two chemicals (5- *vs* 0) and thus on the different osmolarities of their solutions. The labeled erythrocytes were extensively washed with PBS to remove the noninternalized Gd-complexes. The osmolarities of the solutions used were monitored using a manual Löser type 6 Micro-Osmometer. All hematological parameters of interest (number of RBC, Hemoglobin concentration (HGB), Mean Corpuscolar Volume (MCV), Mean Corpuscolar Hemoglobin (MCH), Mean Corpuscolar Hemoglobin Concentration (MCHC)) were evaluated by Emocromocytometric assay on an automated Model MICROS O.T, Horiba ABX Diagnostics hemocytometer and the amount of Hb was evaluated by measuring SORET band region absorbance (413 nm) using a 6715 UV−vis Spectrophotometer Jenway (Bibby Scientific Limited, Staffordshire, U.K.).

ICP-MS Measurements of Metal Content. The number of RBCs was counted at the end of each experiment using the automatic emocromocytometer. Erythrocytes were then destroyed by a strong osmotic shock. Briefly, distillate water was added to the RBC samples (1:50 (v/v)) to give an external osmolarity of *ca.* 60 mOsm/L and samples were agitated to help the lyses. Then, 1 mL of concentrated HNO_3 (70%) was added to 100 μL of each sample which were digested by microwave heating (Milestone MicroSYNTH, Microwave lab station equipped with an optical fiber temperature control and HPR-1000/6 M six position high-pressure reactor, Bergamo, Italy). After digestion, the volume of each sample was brought to 2 mL with ultrapure water, filtered on a 0.4 μm filter and analyzed by ICP-MS, using a Thermo Scientific ELEMENT 2 ICP-MS -Finnigan, Rodano (MI). Three replicates of each sample solution were analyzed. The specimens then underwent ICP-MS analysis to measure the Fe and Gd concentrations.

Depriving Samples of Oxygen. RBCs specimens and Hb solutions were used at normal oxygen pressure (normoxia) and in an oxygen deprived condition (hypoxia), which was obtained by loading the sample in a 5 mm NMR glass tube and inflowing N_2-gas for 30 min. The N_2-flow was gently gurgled inside the specimens by PE-tube to obtain a complete O_2-remotion. The experimental method was tested by observing oxy- and deoxy-Hb amounts *via* the acquisition of Absorbance Spectra on a 6715 UV−vis Spectrophotometer Jenway (Bibby Scientific Limited, Staffordshire, U.K.). Oxy-Hb has two peaks at 541 and 576 nm, while deoxy-Hb has a single peak at 560 nm.

^{1}H-Relaxometric Measurements, NMRD Profiles, and Proton Relaxation Enhancement (PRE) Procedure. The longitudinal water proton relaxation rate was measured on a Stelar Spinmaster (Stelar, Mede, Pavia, Italy) spectrometer operating at 21.5 MHz, by means of the standard inversion−recovery technique. The relaxometric characterization of the field-dependent relaxometry of the Gd-loaded RBCs was achieved using ^{1}H-NMRD profiles. The proton $1/T_1$ NMRD profiles were measured on a fast field-cycling Stelar Relaxometer over a continuum of magnetic field strengths from 0.00024 to 0.47 T (corresponding to 0.01−20 MHz proton Larmor frequencies). Additional data points in the 20−70 MHz range were obtained on a Stelar Spinmaster spectrometer. The binding parameters (affinity constant K_a, number of equivalent and independent binding sites n and the relaxivity of supramolecular adduct Gd-complex/Hb) were determined using the proton relaxation enhancement (PRE) method. The method consists in measuring the R_1 of a Gd complex solution at a fixed concentration by increasing the concentration of the macromolecule. The fitting of the obtained curve furnishes the K_a and R_1^{bound} values. The paramagnetic contribution to the observed relaxation rate of hemoglobin in the PRE experiments was accounted for by the use of premeasured calibration lines obtained by plotting the observed relaxation rate of Hb suspensions at different concentrations *vs* their ICP-MS measured iron content.

Animal Handing. Six to ten week-old female BALB/c mice (Charles River Laboratories Italia s.r.l., Calco, Italy) were subcutaneously inoculated in the left flank with 0.1 mL of a single suspension containing 5×10^5 TS/A mouse breast cancer cells. TS/A cells were grown in a RPMI medium supplemented with 10% FBS, 2 mM glutamine, 100 U/mL penicillin and 100 μg/mL streptomycin. Mice were kept in standard housing in a 12 h light/dark cycle with rodent chow and water available *ad libitum*. Experiments were performed according to national regulations and were approved by the local animal experiment ethical committee. Mice were anesthetized for the MRI experiments by the intramuscular injection of a mixture of Tiletamine/Zolazepam (Zoletil 100, Virbac, Milan, Italy) 20 mg/kg and xylazine (Rompun; Bayer, Milan, Italy) 5 mg/kg. The Gd-labeled RBCs were prepared as described above and injected into the mouse tail vein at a dose of *ca.* 0.04 mmol Gd/kg.

The safety profile of the Gd-labeled RBCs was qualitatively investigated. No immunological reaction was present as the RBCs used for the transfusion were obtained from syngeneic donor mice. Moreover, in order to avoid hypervolemia, a volume of blood, which corresponded to the volume of labeled blood that was to be injected, was removed from the receiving mouse before the administration of the transfusion. Furthermore, the mice were observed for up to 6 months after the injection of Gd-labeled RBCs and no sign of suffering was noted.

MRI Experiments. All MR images were acquired at 7.1 T on a Bruker Avance 300 MHz spectrometer equipped with a micro-imaging probe at room temperature (21 °C). $T_{2\text{-weighted}}$ images were acquired using a standard $T_{2\text{-weighted}}$ Rapid Acquisition with Relaxation Enhancement (RARE) sequence with the following parameters (TR = 5000 ms, TE = 5.5 ms, RARE factor = 32, FOV = 3.5 cm × 3.5 cm, slice thickness = 1 mm, matrix 128 × 128). $T_{1\text{-weighted}}$ images were acquired using a standard $T_{1\text{-weighted}}$ Multi Slice Multi Echo (MSME) sequence with the following parameters (TR = 200 ms, TE = 3.3 ms, number of average = 4, FOV = 3.5 cm × 3.5 cm, slice thickness = 1 mm, matrix 128 × 128, resolution 0.273 × 0.273 mm/pixel). To eliminate the flow artifact, axial saturation slices were applied close to the region of acquisition with the following parameters: slice thickness 20 mm, Hermitian shape pulse, length 1 ms, Flip Angle of 90°. A glass tube containing water as reference was inserted close to the mouse body.

Image Analysis. Tumor volume was determined using multi-slice T_{2w} images. A Region of Interest (ROI) was manually drawn and the slice volume was calculated. The T_{1w} images with the saturation slices were processed using ImageJ software (NIH). The T_1 contrast enhancement (S^{post}) in the ROI upon Gd-DOTP-RBC injection was calculated with respect to the signal measured before Gd-RBC injection (S^{pre}) using the following expression 2:

$$\varepsilon_T^{\text{Gd-DOTP}} = \frac{S^{post} - S^{pre}}{S^{pre}} \quad (2)$$

S^{pre} and S^{post} were normalized with respect to an external reference. The same analysis was carried out on one of the main blood vessels in which the flow artifact T_1 signal was removed by the saturation slices. The ROI was chosen inside the veins where total hemoglobin is expected to be in the deoxygenated state (eq 3).

$$\varepsilon_V^{\text{Gd-DOTP}} = \frac{S_v^{post} - S_v^{pre}}{S_v^{pre}} \quad (3)$$

S_v^{pre} and S_v^{post} were normalized with respect to same external reference as before.

The ratio (R_{GdDOTP}) between the SE inside the tumor voxels and the mean SE in the vein was calculated according to the following expression (eq 4):

$$R_{GdDOTP} = \frac{\varepsilon_T^{\text{Gd-DOTP}}}{\varepsilon_V^{\text{Gd-DOTP}}} \quad (4)$$

The images acquired upon Gd-HPDO3A-RBC administration were analogously analyzed and the ratio ($R_{GdHPDO3A}$) between SE inside the tumor voxels and the mean SE in the main vessel was calculated according to the following expression (eq 5):

$$R_{GdHPDO3A} = \frac{\varepsilon_T^{\text{Gd-HPDO3A}}}{\varepsilon_V^{\text{Gd-HPDO3A}}} \quad (5)$$

The obtained maps report on vascular volume (V_v) voxel per voxel.

The images obtained upon Gd-DOTP-RBC and Gd-HPDO3A-RBC administration were combined as follows (eq 6), in order to obtain normalized maps that report the oxygenation state independently from the actual vessel density in the voxel:

$$\text{Deoxygenation Index (DI)} = \frac{R_{\text{GdDOTP}}}{R_{\text{GdHPDO3A}}} \quad (6)$$

A relative oxygenation index (OI%) was calculated from this value as follows (eq 7):

$$\text{OI}\% = (1 - \text{DI}) \times 100 \quad (7)$$

Microscopy. Mice were sacrificed after MRI and PAI acquisition and TS/A-derived tumors were explanted. Tumors were washed twice in PBS (Sigma-Aldrich, Milano, Italy) and embedded in Optimal Cutting Temperature compound (OCT, from Bio-Optica, Milano, Italy) prior to being frozen. Three micrometer thick sections were cut with a microtome-cryostat along the entire tumor and two equivalent series of glass slides were prepared. Sections were acetone fixed for 10 min at room temperature, rinsed twice in PBS and immediately blocked in PBS + bovin serum albumin (BSA) 10% for 30 min at room temperature. Slices were then incubated overnight with mouse anti-HIF1α (Santa Cruz, CA) and rat anti-CD31 (BD Pharmingen, Milan, Italy) primary antibodies. After extensive washes in PBS 10% BSA, sections were incubated for 1 h at room temperature with Alexa Fluor 568 goat anti-rat and Alexa Fluor 488 goat anti-mouse secondary antibodies, both from Life Technologies (Carlsbad, CA). Glasses were then washed again, incubated with DAPI (DakoCytomation) for 15 min at room temperature and mounted in Faramount aqueous mounting medium (Sigma-Aldrich). Images were acquired using an ApoTome system equipped with AxioVision Release 4.8 software (Zeiss, Germany).

Photoacoustic Detection of Vascular Volume. PA (photoacoustic) images were acquired using a VisualSonics Vevo 2100 LAZR Imaging Station (VisualSonics, Inc., Toronto, Canada). Hair was removed from areas of interest using a depilatory cream and Ultrasound gel was applied. To collect anatomical information at high resolution, B-mode imaging was acquired using a high-frequency ultrasound probe (MS550D, VisualSonics, Canada; broadband frequency, 22−55 MHz; image axial resolution, 40 μm) at 40 MHz. Oxygen saturation and hemoglobin concentration were measured at 21 MHz frequency (LZ250, VisualSonics, Canada). Hb content was measured with a laser set at 812 nm. Oxygen saturation (SO_2 %) was measured with PA dual-wavelength imaging at 750 and 850 nm. All PA images were co-registered with gray scale B-mode images. The quantification of total hemoglobin and oxygen saturation was achieved using HemoMeaZure tool and OxyZated tool (VisualSonics, Canada), respectively.

Statistical Analysis. Data are represented as mean ± SD. A paired two-tail Student's *t* test was used in the comparison of PAI data in the *pre* and *post* Gd-DOTP-RBC administration experiment and in the comparison of MRI data in the *early* and *late* stage tumor progression experiment.

Conflict of Interest: The authors declare no competing financial interest.

Supporting Information Available: The Supporting Information is available free of charge on the ACS Publications website at DOI: 10.1021/acsnano.5b02604.

Loading of Gd-HPDO3A and Gd-DOTP inside RBCs; absorption spectra of oxy- and deoxy-Hb; PAI O_2 measurement pre and post Gd-DOTP administration; comparison of oxygen content evaluated using MRI and PAI; comparison of early and late stage tumors (PDF)

Acknowledgment. This research was funded by the AIRC Investigator Grant IG2013-14565 and by the EU COST Action TD1004. E.D.G. acknowledges the support of Fondazione Veronesi for the assignment of her Fellowship.

REFERENCES AND NOTES

1. Gillies, R. J.; Gatenby, R. A. Hypoxia and Adaptive Landscapes in the Evolution of Carcinogenesis. *Cancer Metastasis Rev.* **2007**, *26*, 311–317.
2. Jain, R. K. Determinants of Tumor Blood Flow: a Review. *Cancer Res.* **1988**, *48*, 2641–2658.
3. Vaupel, P.; Harrison, L. Tumor hypoxia: Causative Factors, Compensatory Mechanisms, and Cellular Response. *Oncologist* **2004**, *9*, 4–9.
4. Brown, J. M. Tumor Hypoxia in Cancer Therapy. *Methodsn Enzymol.* **2007**, *435*, 297–302.
5. Tatum, J. L.; Kelloff, G. J.; Gillies, R. J.; Arbeit, J. M.; Brown, J. M.; Chao, K. S.; Chapman, J. D.; Eckelman, W. C.; Fyles, A. W.; Giaccia, A. J.; et al. Int. Hypoxia: Importance in Tumor Biology, Noninvasive Measurement by Imaging, and Value of its Measurement in the Management of Cancer Therapy. *Int. J. Radiat. Biol.* **2006**, *82*, 699–757.
6. Brown, J.M R.; Wilson, W. Exploiting Tumor Hypoxia in Cancer Treatment. *Nat. Rev. Cancer* **2004**, *4*, 437–447.
7. Hockel, M.; Vaupel, P. Tumor Hypoxia: Definitions and Current Clinical, Biologic, and Molecular Aspects. *J. Natl. Cancer Inst.* **2001**, *93*, 266–276.
8. Krohn, K. A.; Link, J. M.; Mason, R. P. Molecular Imaging of Hypoxia. *J. Nucl. Med.* **2008**, *49*, 129S–1485.
9. Vaupel, P.; Schlenger, K.; Knoop, C.; Hockel, M. Oxygenation of Human Tumors: Evaluation of Tissue Oxygen Distribution in Breast Cancers by Computerized O_2 Tension Measurements. *Cancer Res.* **1991**, *51*, 3316–3322.
10. Kavanagh, M. C.; Sun, A.; Hu, Q.; Hill, R. P. Comparing Techniques of Measuring Tumor Hypoxia in Different Murine Tumors: Eppendorf pO2 Histograph, [3H]Misonidazole Binding and Paired Survival Assay. *Radiat. Res.* **1996**, *145*, 491–500.
11. Piao, W.; Tsuda, S.; Tanaka, Y.; Maeda, S.; Liu, F.; Takahashi, S.; Kushida, Y.; Komatsu, T.; Ueno, T.; Terai, T.; et al. Development of Azo-Based Fluorescent Probes to Detect Different Levels of Hypoxia. *Angew. Chem., Int. Ed.* **2013**, *52*, 13028–13032.
12. Shao, Q.; Morgounova, E.; Jiang, C.; Choi, J.; Bischof, J.; Ashkenazi, S. *In Vivo* Photoacoustic Lifetime Imaging of Tumor Hypoxia in Small Animals. *J. Biomed. Opt.* **2013**, *18*, 076019.
13. Padhani, A. PET Imaging of Tumor Hypoxia. *Cancer Imaging* **2006**, *6*, S117–S121.
14. Baskin, A.; Buchegger, F.; Seimbille, Y.; Ratib, O.; Garibotto, V. PET Molecular Imaging of Hypoxia in Ischemic Stroke: an Update. *Curr. Vasc. Pharmacol.* **2013**, *13*, 1570–1611.
15. Caravan, P.; Ellison, J. J.; McMurry, T. J.; Lauffer, L. B. Gadolinium(III) Chelates as MRI Contrast Agents: Structure, Dynamics, and Applications. *Chem. Rev.* **1999**, *99*, 2293–2352.
16. Do, Q. N.; Ratnakar, J. S.; Kovács, Z.; Sherry, A. D. Redox- and Hypoxia-Responsive MRI Contrast Agents. *ChemMedChem* **2014**, *9*, 1116–1129.
17. Price, J. M.; Robinson, S. P.; Koh, D. M. Imaging Hypoxia in Tumors with Advanced MRI. *Q. J. Nucl. Med. Mol. Imaging* **2013**, *57*, 257–270.
18. Lu, H.; van Zijl, P. C. Experimental Measurement of Extravascular Parenchymal BOLD Effects and Tissue Oxygen Extraction Fractions Using Multi-echo VASO fMRI at 1.5 and 3.0 T. *Magn. Reson. Med.* **2005**, *53*, 808–816.
19. Krohn, K. A.; Link, J. M.; Mason, R. P. Molecular Imaging of Hypoxia. *J. Nucl. Med.* **2008**, *49*, 129S–148.
20. Aime, S.; Botta, M.; Gianolio, E.; Terreno, E. A p(O(2))-Responsive MRI Contrast Agent Based on the Redox Switch of Manganese(II/III) - Porphyrin Complexes. *Angew. Chem., Int. Ed.* **2000**, *39*, 747–750.
21. Robinson, S. P.; Griffiths, J. R. Current Issues in the Utility of 19F Nuclear Magnetic Resonance Methodologies for the Assessment of Tumor Hypoxia. *Philos. Trans. R. Soc., B* **2004**, *359*, 987–996.
22. Shi, Y.; Oeh, J.; Eastham-Anderson, J.; Yee, S.; Finkle, D.; Peale, F. V., Jr; Ross, J.; Hedehus, M.; van Bruggen, N.; Venook, R.; et al. Mapping *in Vivo* Tumor Oxygenation within Viable Tumor by 19F-MRI and Multispectral Analysis. *Neoplasia* **2013**, *15*, 1241–1450.

23. Laustsen, C.; Lycke, S.; Palm, F.; Østergaard, J. A.; Bibby, B. M.; Nørregaard, R.; Flyvbjerg, A.; Pedersen, M.; Ardenkjaer-Larsen, J. H. High Altitude May Alter Oxygen Availability and Renal Metabolism in Diabetics as Measured by Hyperpolarized [1-(13)C]Pyruvate Magnetic Resonance Imaging. *Kidney Int.* **2014**, *86*, 67–74.
24. Pacheco-Torres, J.; López-Larrubia, P.; Ballesteros, P.; Cerdán, S. Imaging Tumor Hypoxia by Magnetic Resonance Methods. *NMR Biomed.* **2011**, *24*, 1–16.
25. Aime, S.; Ascenzi, P.; Comoglio, E.; Fasano, M.; Paoletti, S. Molecular Recognition of R-and T-State of Human Adult Hemoglobin by a Paramagnetic Gd(III) Complexes by Means of the Measurement of Solvent Water Proton Relaxation Rate. *J. Am. Chem. Soc.* **1995**, *117*, 9365–9366.
26. Aime, S.; Fasano, M.; Paoletti, S.; Bellelli, A.; Coletta, M.; Ascenzi, P. Stabilization of the T-State of Ferrous Human Adult and Fetal Hemoglobin by Ln(III) Complexes: a Thermodynamic Study. *J. Inorg. Biochem.* **1998**, *71*, 37–43.
27. Aime, S.; Digilio, G.; Fasano, M.; Paoletti, S.; Arnelli, A.; Ascenzi, P. Metal Complexes as Allosteric Effectors of Human Hemoglobin: an NMR Study of the Interaction of the Gadolinium(III) bis(m-boroxyphenylamide)diethylenetriaminepentaacetic Acid Complex with Human Oxygenated and Deoxygenated Hemoglobin. *Biophys. J.* **1999**, *76*, 2735–2743.
28. Yuan, Y.; Tam, M. F.; Simplaceanu, V.; Ho, C. New Look at Hemoglobin Allostery. *Chem. Rev.* **2015**, *115*, 1702–1724.
29. Lukin, J. A.; Kontaxis, G.; Simplaceanu, V.; Yuan, Y.; Bax, A.; Ho, C. Quaternary Structure of Hemoglobin in Solution. *Proc. Natl. Acad. Sci. U. S. A.* **2003**, *100*, 517–520.
30. Ferrauto, G.; Delli Castelli, D.; Di Gregorio, E.; Langereis, S.; Burdinski, D.; Grüll, H.; Terreno, E.; Aime, S. Lanthanide-Loaded Erythrocytes as Highly Sensitive Chemical Exchange Saturation Transfer MRI Contrast Agents. *J. Am. Chem. Soc.* **2014**, *136*, 638–641.
31. Johnson, K. M.; Tao, J. Z.; Kennan, R. P.; Gore, J. C. Gadolinium-Bearing Red Cells as Blood Pool MRI Contrast Agents. *Magn. Reson. Med.* **1998**, *40*, 133–142.
32. Ferrauto, G.; Di Gregorio, E.; Dastrù, W.; Lanzardo, S.; Aime, S. Gd-Loaded-RBCs for the Assessment of Tumor Vascular Volume by Contrast-Enhanced-MRI. *Biomaterials* **2015**, *58*, 82–92.
33. Di Gregorio, E.; Ferrauto, G.; Gianolio, E.; Aime, S. Gd Loading by Hypotonic Swelling: an Efficient and Safe Route for Cellular Labeling. *Contrast Media Mol. Imaging* **2013**, *8*, 475–486.
34. Di Gregorio, E.; Gianolio, E.; Stefania, R.; Barutello, G.; Digilio, G.; Aime, S. On the Fate of MRI Gd-Based Contrast Agents in Cells. Evidence for Extensive Degradation of Linear Complexes upon Endosomal Internalization. *Anal. Chem.* **2013**, *85*, 5627–5631.
35. Terreno, E.; Terreno, E.; Geninatti Crich, S.; Belfiore, S.; Biancone, L.; Cabella, C.; Esposito, G.; Manazza, A. D.; Aime, S. Effect of the Intracellular Localization of a Gd-Based Imaging Probe on the Relaxation Enhancement of Water Protons. *Magn. Reson. Med.* **2006**, *55*, 491–497.
36. Strijkers, G. J.; Hak, S.; Kok, M. B.; Springer, C. S.; Nicolay, K. Three-Compartment T1 Relaxation Model for Intracellular Paramagnetic Contrast Agents. *Magn. Reson. Med.* **2009**, *61*, 1049–1058.
37. Kok, M. B.; Hak, S.; Mulder, W. J.; van der Schaft, D. W.; Strijkers, G. J.; Nicolay, K. Cellular Compartmentalization of Internalized Paramagnetic Liposomes Strongly Influences both T_1 and T_2 Relaxivity. *Magn. Reson. Med.* **2009**, *61*, 1022–1032.
38. Gerling, M.; Zhao, Y.; Nania, S.; Norberg, K. J.; Verbeke, C. S.; Englert, B.; Kuiper, R. V.; Bergström, A.; Hassan, M.; Neesse, A.; et al. Real-Time Assessment of Tissue Hypoxia *in Vivo* with Combined Photoacoustics and High-Frequency Ultrasound. *Theranostics* **2014**, *4*, 604–613.
39. Shao, Q.; Morgounova, E.; Jiang, C.; Choi, J.; Bischof, J.; Ashkenazi, S. *In Vivo* Photoacoustic Lifetime Imaging of Ttumor Hypoxia in Small Animals. *J. Biomed. Opt.* **2013**, *18*, 076019.
40. Nanni, P.; De Giovanni, C.; Lollini, P. L.; Nicoletti, G.; Prodi, G. TS/A: a New Metastasizing Cell Line from a BALB/c Spontaneous Mammary Adenocarcinoma. *Clin. Exp. Metastasis* **1983**, *1*, 373–380.
41. Baudelet, C.; Gallez, B. How Does BOLD Contrast Correlate with Oxygen Partial Pressure (pO_2) Inside Tumors? *Magn. Reson. Med.* **2002**, *48*, 980–986.
42. Mendichovszky, I.; Jackson, A. *Br. J. Radiol.* **2011**, *84*, S145–S158.
43. Li, X.; Zhang, S.; Zhao, P.; Kovacs, Z.; Sherry, A. D. Synthesis and NMR Studies of New DOTP-Like Lanthanide(III) Complexes Containing a Hydrophobic Substituent on One Phosphonate Side Arm. *Inorg. Chem.* **2001**, *40*, 6572–6579.